Int. J. Electrochem. Sci., 14 **(2019)** 2539– 2559, doi: 10.20964/2019.03.08

International Journal of ELECTROCHEMICAL SCIENCE
www.electrochemsci.org

The Corrosion Behavior of C-steel, Al-alloy and Pure-Cu in Red Oak Wood Extract: A Comparative Study

Ehteram A. Noor[1, 2], *Azza A. Al-Ghamdi*[1, 2], *Mohamed Abdel Salam*[1*]

[1]Chemistry Department, Faculty of Science, King Abdulaziz University, P.O Box 80200-Jeddah 21589, Kingdom of Saudi Arabia
[*]E-mail: masalam16@hotmail.com, mabdelsalam@kau.edu.sa

[2]Chemistry Department, Faculty of Science, University of Jeddah, P.O. Box 80327, Jeddah 21589, Saudi Arabia

Received: 15 October 2018/ *Accepted:* 5 December 2018 / *Published:* 7 February 2019

The corrosion behavior of three metals (C-steel, Al-alloy, and Pure-Cu) in the red oak wood extract (ROWE) had been studied using weight loss (expressed as thickness loss), potentiodynamic polarization and electrochemical impedance spectroscopy. Visual and microscopic inspection of the corrosion systems was done using optical photography and SEM techniques. The results revealed that the thickness loss data fit well the kinetic power law relation ($\rho = Kt^n$). Depending on both values of thickness loss of one year and the instantaneous corrosion rate, the studied metals gave the following order of corrosion: C-steel > Al-alloy > Pure-Cu. Good correlation between this order and the color and clarity of the metal/ROWE corrosion systems was obtained, where C-steel/ROWE showed the highest change in color and turbidity through the corrosion duration. Pure-Cu gave the lowest value for corrosion rate with exponent n < 0.5 indicating good protective properties for the corrosion product layer which showed a compact structure with no detection for microbial activity. Open structure corrosion layer (n > 0.5) with microbial activity was observed for both C-steel and Al-alloy which distributed generally on the surface of the former while locally on the surface of the latter. Various electrochemical parameters were estimated and discussed. Finally, good agreement between the results obtained from various techniques confirming that C-steel gives the highest corrosion rate while the lowest corrosion rate was recorded for Pure-Cu.

Keywords: Corrosion; Impedance; Metals, Polarization; Wood; Thickness loss

1. INTRODUCTION

Wood has been one of the oldest standing building materials in human life throughout history. It has been played an important role both for building and manufacture of furniture, weapons, and tools. According to human life development, the metallic materials such as steel and bronze had been used widely as essential building materials. However, wood continues to build simple constructions and

amazing structures. It is well known that wood and metal are used jointly for many purposes, so they are highly well-suited materials. Unfortunately, corrosion problems occur under certain conditions and hence destroys the compatible wood-metal relationship, and as a result, both metal and wood will be damaged with time. Wood is classified as corrosive material because of the natural production of acetic acid from wood material giving a slightly acidic environment which accelerates the corrosion process [1]. Acetic acid is one of the most corrosive agencies known and attack most metals [2]. Wood humidity (water content) play an important role for both (i) acetic acid production and (ii) corrosion process. The former needs water molecules of wood hydrolysis to produce acetic acid [2] and the latter needs an aqueous bath for electrical conductance, i.e., corrosion is an electrochemical process [3]. In dry wood, water is not free and is present only in the cell walls, and within the cells, hence it is not available to accelerate the corrosion process [4]. However, corrosion by wood is a complex phenomenon with a multitude of variables involved. The risk of corrosion by wood depends on wood moisture content, wood species, the presence of external contaminants, wood condition (untreated or treated with definite preservative or flame-retardant substances) and metal type. The relative importance of variables changes with different materials, so no universal guide to corrosion by wood would obtain. Recently, several studies had been done by Zelinka et al. [5-13] and Kear et al. [14-16] to understand the metal corrosion by wood and/or wood extract under various conditions of treatment.

The present work aimed to study the corrosion behavior of some metals (carbon steel, C-steel; aluminum alloy, Al-alloy; and Pure copper, Pure-Cu) in red Oak wood extract (ROWE) using weight loss (WL) and electrochemical measurements (potentiodynamic polarization, PDP, and electrochemical impedance spectroscopy, EIS). Visual and microscopic examination of the surface morphology of the studied metals were evaluated and discussed.

2. EXPERIMENTAL

2.1. Materials

Three metals were tested: C-steel, Al-alloy, and Pure-Cu (99.99%). The chemical composition of C-steel and Al-alloy are given in Table 1. The tested specimens were cut to rods with size depends on the applied technique. A commercially Red Oak Wood board, 250 mm by 50 mm by 1.5 m was purchased from “Wood World Trading Co.” member of CHABROS INTERNATIONAL GROUP. They have reported that red oak wood (ROW) material originated from Queensland, Australia, with detailed technical data includes a general description, mechanical properties, durability and uses of ROW but no information about the treatment process. They only mentioned that the heartwood is resistant to preservative treatment, and the sapwood permeable. The Wood board was ground mechanically into sawdust. The collected sawdust was stored in a dry plastic bag at room temperature.

2.2. Methods

2.2.1. Preparation of red oak wood extract (ROWE)

The best conditions for extraction were reported by Zelinka et al. [5]. The ratio of sawdust to

water was 1:10 (weight basis) and the extraction period was one week at room temperature. After the extraction period, the solid wood phase was separated out, and the extract was stored at 4°C to reduce biological activity for the duration of storage.

Table 1. Composition of C-steel, Al-alloy and Pure-Cu (wt%).

Specimens	Elemental composition (wt%)							
C-steel	C	Mn	Si	S	Cu	N	Fe	
	0.12	0.69	0.19	0.02	0.06	0.05	remainder	
Al alloy	Si	Fe	Cu	Mn	Mg	Zn	Ti	Al
	1.00	0.27	0.04	0.93	0.93	0.02	0.01	remainder

2.2.2. Analysis of ROWE

The average values for a duplicated measurement for the physicochemical parameters of ROWE were determined by the Saudi Geological Survey (SGS) using Atomic Absorption Spectrometer for all cations, Mettler Toledo DL25 autotitrator for chloride and bicarbonate ions and WTW (Photo-lap spectral) for phosphate, nitrate and sulfate ions. Table 2 illustrates the Physicochemical parameters (salt content, pH, conductivity) of the studied OWE. The extremely low value of Cu^{2+} ions concentration indicates that the studied wood was untreated**.**

Table 2. The physicochemical parameters for ROWE.

Salts content ($mg.L^{-1}$)										
Cu^{2+}	Ca^{2+}	Mg^{2+}	K^{+}	Na^{+}	NH_4^{+}	Cl^{-1}	HCO_3^{-}	SO_4^{2-}	PO_4^{3-}	NO_3^{-}
0.27	11.60	5.04	63.33	2.20	0.09	3.00	< 4.00	20.00	30.00	85.00
	pH				Conductivity ($\mu s.cm^{-1}$)					
	4.24				282.00					

2.2.3. Pretreatment of metal specimens

For all the experiments, the studied specimens were pre-treated before the experiments by polishing successively with emery paper (SiC) of different grades up to 1200, then washed thoroughly with de-ionized water, degreased with ethanol and finally dried at room temperature with a stream of air.

2.2.4. WL method

The experiments were carried out at the room temperature of 22 ± 1 °C. A constant volume (70 mL) of ROWE was placed in well-closed glass bottles (Figure 1) and were left at room temperature for 20 min to achieve thermal equilibrium with the surrounding environment. The clean, dried specimens (1 cm in diameter and 5 cm in length) were weighed (W_1, g) using a digital balance of 10^{-4} g accuracy and

each specimen was inserted carefully in the studied ROWE. The total duration of the experiment was 15 weeks. The specimens were investigated after 1, 2, 3, 5, 7, 10 and 15 weeks of the ROWE exposure. At each time interval, the specimens were removed from the studied solution and roughly washed with water and brush. After that, the sticky corrosion products were removed at room temperature using pickling solutions (Table 3) according to ASTM G 1-90 [17]. Then the specimens were rinsed with ethanol and dried with air and finally weighed (W_2, g). Weight loss was expressed as thickness loss (ρ, µm) according to the following equation [18]:

$$\rho\ (\mu m) = \frac{W_2 - W_1}{A \times d} \times 10^4 \quad (1)$$

Where A is the specimen surface area (cm^2), d is metal density ($g.cm^{-3}$), and 10^4 is conversion factor.Each experiment was run twice and the average value was taken.The values of precision for thickness loss of C-steel, Al-alloy, and Pure-Cu are ± 0.37, ± 0.05 and ± 0.01 µm, respectively.

Figure 1. The blank of ROWE.

Table 3. The used pickling solutions.

Metal type	Pickling solution	Time of pickling
C-steel	50 g sodium hydroxide (NaOH) 200 g granulated zinc, reagent water to make 1000 mL	1 min
Al-alloy	Nitric acid (HNO_3, sp gr 1.42)	1 min
Pure-Cu	100 mL sulfuric acid (H_2SO_4, sp gr 1.84), reagent water to make 1000 mL	1 min

2.2.5. Electrochemical methods

Electrochemical measurements were performed with ACM Gill AC (model 655) potentiostat/galvanostat operated with Power suite software. The electrochemical tests in ROWE were

carried out using a three-electrode cell system. The working electrodes were C-steel, Al-alloy and pure-Cu specimens (1 cm in diameter and 5 cm in length). Each specimen was inserted in Teflon tube of suitable diameter and was fixed with chemical resistance adhesive, so constant surface area (0.785 cm^2) exposed to the tested solution. The platinum wire and $Ag/AgCl_{(s)}/KCl_{saturated(aq)}$ served as the counter and reference electrodes, respectively. All studied systems were stagnant, naturally aerated and maintained at 30 ºC.The EIS measurements were carried out after one h of immersion in the studied solution to reach steady state potential. The covered frequency range was 100 kHz to 0.1 Hz with a 30 mV sinusoidal applied potential. Spectral analyses were performed using ZSimDemo 3.20 software. Potentiodynamic polarization curves were drawn immediately after EIS measurements starting from cathodic potentials and ending at anodic potentials with respect to the corrosion potential (E_{corr} *vs.* $Ag/AgCl_{(s)}/KCl_{saturated(aq)}$) at a sweep rate of 1 mV/s. The range between cathodic and anodic potentials varied according to the type of the working electrode. Potentiodynamic polarization parameters for the corrosion of the studied specimens were estimated using analysis software of ACM Gill 1070 by applying Tafel ruler working by extrapolation method. Each experiment was run twice and the average value was taken.

2.2.6. Visual inspection and scanning electron microscopy (SEM)

Visual inspection of an object can be accomplished in simply when there is physical access to this purpose. Visual inspection of the corrosion reaction vessels was done at different periods of immersion using optical photographs to follow solution color change and the density of corrosion products which precipitate through the experiment duration. The type of corrosion, such as general corrosion and/or localized (pitting) corrosion was also inspected using optical photographs of the studied specimens before and after pickling at different periods of immersion in ROWE. The surface morphology of specimens after ten weeks exposure to the ROWE without pickling treatment was studied using SEM technique (Quanta FEG 450).

3. RESULTS AND DISCUSSION

3.1. Visual Inspection of metal/ROWE corrosion systems

Figure 2 represents naked-eye visual inspection for color and clarity of the ROWE after becomes in contact with the studied specimens for different immersion periods at room temperature. The ROWE which contains C-steel specimen was observable in color change and turbidity more than in the case of Al-alloy and pure-Cu (Figure 2) as all compared to the blank ROWE solution (Figure. 1). The very dark blue solution was observed in the first week of C-steel immersion in ROWE even the specimen not clearly detected through the solution. However, the dark blue color was detected dramatically through the duration of 60 min of immersion as illustrated in Figure 3. With increasing immersion time, a black precipitate was accumulated in the bottom, and the wall of the experiment bottle and this precipitate becomes denser at the tenth week while the solution is losing its dark color as compared to the first week but still has turbidity appearance. Zelinka and stone observed the similar blue/black cloud of visible

precipitate around the steel electrode after the polarization resistance test in oak wood extract [8]. On the other hand, the color of ROWE did not change appreciably in the case of Al-alloy specimen as compared with the blank solution while white precipitate appears with extended immersion periods for more than one week. Unfortunately, the localized attack was observed on the Al-alloy surface, since brownish materials accumulated around the specific area rather than the rest of the metal surface. Finally, the ROWE containing Pure-Cu specimen has no turbidity appearance even at long immersion (10 weeks) but somewhat it becomes darker than the blank solution. The previous observations in the three studied metal/ROWE systems may be related to the interaction between the dissolved metal ion and the constituents of ROWE. Since ROWE was prepared in water, the interpretation for the previous observations must be based on the water-soluble (hydrophilic fraction) contents of ROWE. It was reported that hydrophilic fraction of wood, extractable with water contains large amounts of phenolic constituents such as condensed tannins which often called phenolic acids [19]. Most tannins have several o-diphenol groups and thus have chelating ability facilitates forming complexes with many metal ions such as $Fe^{2+,}$ Fe^{3+}, Cu^{2+}, Zn^{2+}, Cd^{2+}, Pb^{2+} or Al^{3+} [20-24]. Tannin/metal complexes regularly precipitate in aqueous solutions [25]. There is evidence that as the complexes with the ferrous iron oxidize, ferric ions are released, and black ferric tannate is precipitated [20] which confirmed the black material that obviously was observed in the C-steel/ROWE system (Figure 2 and Figure 3). Since tannin/Al^{3+} complexes are colorless [26], this may be explained the white precipitate in the Al-alloy/ROWE system (Figure 2). However, no obvious solid material was observed in the Pure-Cu/ROWE system even at tenth week of immersion which may be attributed to soluble complex formation under the studied conditions. The previous observations confirmed that C-steel, Al-alloy, and Pure-Cu were corroded (dissolved) under the influence of ROWE, but not adequate to discuss the corrosion susceptibility of the three specimens. Hence numerical values for the corrosion rates must be needed.

3.2. WL measurements at room temperature

3.2.1. Corrosion kinetics

Figure 4 shows the thickness loss of C-steel, Al-alloy, and Pure-Cu immersed in ROWE at room temperature for different immersion time. The thickness loss increased gradually with exposure time, and the resultant curves are reminiscent of the typical plot of parabolic laws or power functions. Thus, the corrosion data obtained for the studied metals can be fitted to the kinetic power model:

$$\rho = Kt^n \quad (2)$$

where K and n are constants. However, a power model involving the logarithmic transformation of the immersion time and thickness loss must be applied to obtain the linear form of the above equation as follows:

$$\log \rho = \log K + n \log t \quad (3)$$

The power model is broadly used to predict corrosion behavior of metallic materials even after long intervals of immersion, and its precision and consistency have been verified by several authors [18, 27-31]. If the power model (Eq. 3) is satisfied, corrosion behavior will evidently be described by only

two parameters thickness loss (K) after the first year of immersion ($t = 1y$) and the time exponent n.

Figure 2. Optical photographs for ROWE/metal systems for different immersion times at room temperature (22 ± 1 °C).

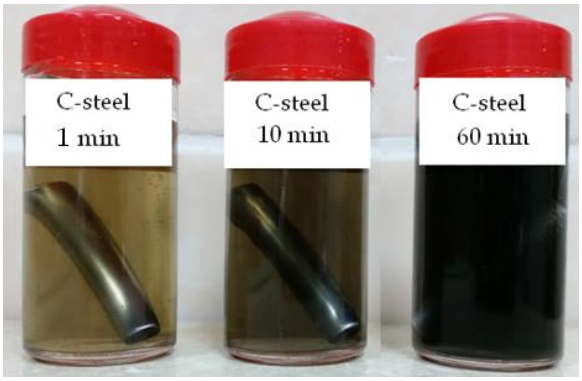

Figure 3. The change of color and turbidity for ROWE/C-steel system during 60 min of immersionat room temperature (22 ± 1 °C).

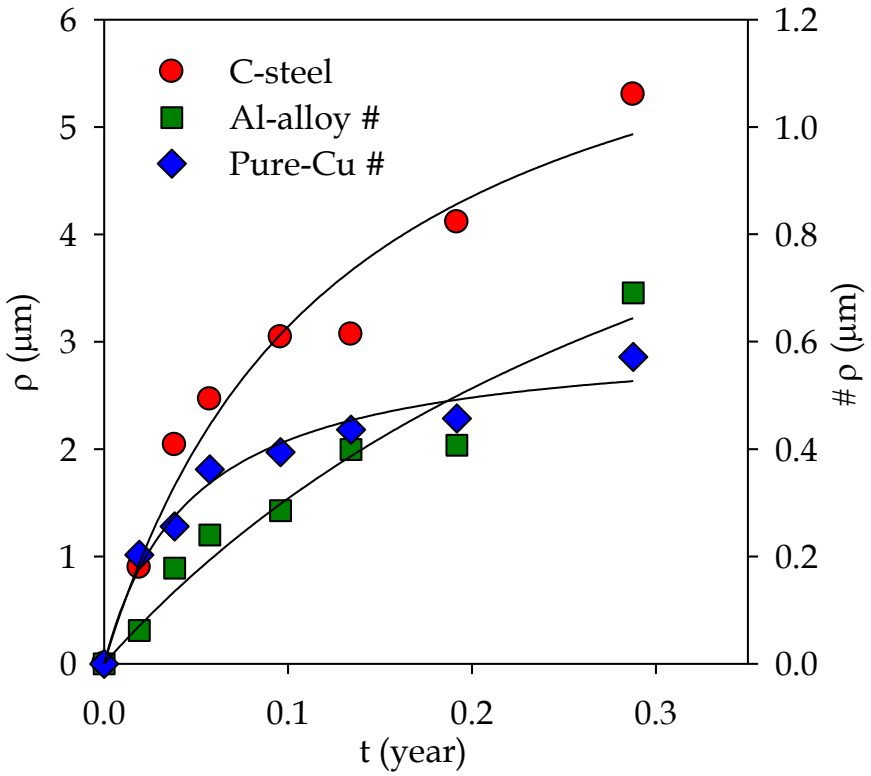

Figure 4. Thickness loss of the studied metals as a function of immersion time in ROWE at room temperature (22 ± 1 °C).

The value of exponent n can serve as an investigative tool to indicate the diffusion properties through the corrosion products that formed on the metal surface, and the following situations can be obtained [32]:

(i) With n close to 0.5, the corrosion process is controlled by diffusion through the corrosion products that remain on the metal surface.

(ii) With n more than 0.5, the diffusion process is accelerated due to corrosion products detachment by dissolution, soluble complex formation, flaking, etc.

(iii) With n less than 0.5, compact and protective layer formed on the metal surface which led to a decrease in the diffusion coefficient with time.

Generally, n < 1. In the special case when n = 1, Eq. 2 becomes linear ($\rho = Kt$) and the thickness loss of one-year immersion equal to the slope of the relation. An n value > 1 would indicate that the corrosion rate increased with immersion time [33].

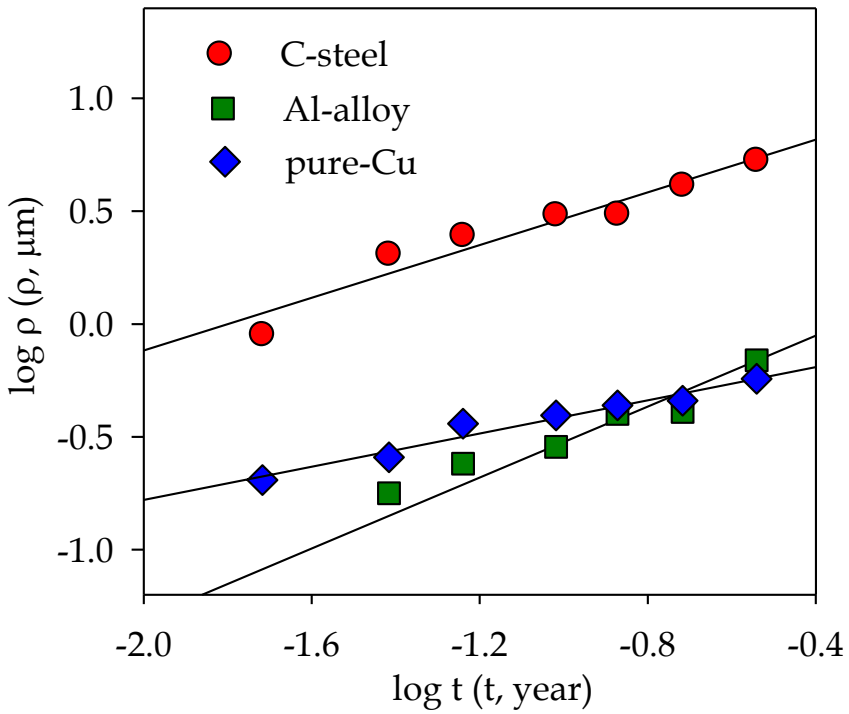

Figure 5. Log-log plots of thickness loss of the studied metals against immersion time in ROWE at room temperature (22 ± 1 °C).

Figure 5 illustrates that the thickness loss data of C-steel, Al-alloy and Pure-Cu in ROWE at room temperature fit well the power kinetic model (Eq. 3) and the fitting expression and correlation coefficients (r^2) are given in Table 4. According to the obtained values of the thickness loss for the first year of immersion (*K*), the corrosion behavior of the studied metals can be given in the following order:

C-steel > Al-alloy > Pure-Cu

The above order is in good agreement to what observed visually in the studied metal/ROWE corrosion systems (Figure 2) where C-steel/ROWE systems showed the highest turbidity through the duration of the experiment.

Since the corrosion process is electrochemical in nature, the studied metal atoms are oxidized to the ionic form in accordance with the following reactions [29]:

$$Cu \rightarrow Cu^{2+} + 2e^- \qquad E^o_{Cu^{2+}/Cu} = +337 \text{ mV} \qquad (4)$$

$$Fe \rightarrow Fe^{2+} + 2e^- \qquad E^o_{Fe^{2+}/Fe} = -440 \text{ mV} \qquad (5)$$

$$Al \rightarrow Al^{3+} + 3e^- \qquad E^o_{Al^{3+}/Al} = -1662 \text{ mV} \qquad (6)$$

Table 4. Fitting expression and kinetic parameters for C-steel, Al-alloy and Pure-Cu corrosion in ROWE at room temperature (22 ± 1 °C).

Metal type	Fitting expression $\log \rho = \log K + n \log t$	N	r^2
C-steel	$\log \rho = \log 11.25 + 0.58 \log t$	0.58	0.93
Al-alloy	$\log \rho = \log 1.83 + 0.79 \log t$	0.79	0.94
Pure-Cu	$\log \rho = \log 0.90 + 0.37 \log t$	0.37	0.96

The standard electrode potentials ($e^{o}_{M^{Z+}/M}$) represents the metal tends to act either as an electron donor (more negative potentials) or electron acceptor (more positive potentials). Pure-Cu gives the lowest corrosion rate, and at the same time, the *n* value (0.37) is less than 0.5 and both results agree well with its standard electrode potential. The strong protective behavior of the film formed on the Cu surface may also be related to the tannins content of ROWE. Beccaria and Mor [34] studied the inhibitive action of tannic acid against the corrosion of Cu in acid solutions. The results revealed that tannic acid behaves as a mixed inhibitor due to the formation of an oxidized compound that is adsorbed either chemically or physically on the Cu surface. On the other hand, C-steel and Al-alloy show another behavior. In general, n value for both C-steel (n = 0.58) and Al-alloy (n = 0.79) are more than 0.5 indicating layer of corrosion products has appreciable diffusion coefficient. Although Al has the highest active standard electrode potential, its alloy gives lower corrosion rates than C-steel. This behavior of both metals could be related to the electrochemical properties of the native oxide film formed naturally on the metal surface. The poor quality of natural iron oxides as compared to the dense, compact Al oxides gives a reasonable explanation for the active behavior of C-steel. Iron oxides flake off almost as soon as it forms, hence a fresh metal surface was exposed to further dissolution and assistant loss of weight. The interesting result was obtained that the lower value of n (corrosion products of less porosity) is associated with C-steel (high corrosion rate) while the reverse trend is obtained for Al-alloy (low corrosion rate and high n value). The visual inspection for ROWE through the duration of metals immersion may support this result. Localized (pitting) attack on the Al-alloy surface is clear-cut (Figure 2). A study by Ricker [33] revealed that the nucleation of pitting after some immersion period longer than the first or second retrieval could increase the *n* value.

3.2.2. Corrosion rate measurements

The average corrosion rate (R_a, $\mu.y^{-1}$) was calculated using the following equation [34]:

$$R_a = \frac{\rho_i - \rho_{i-1}}{t_i - t_{i-1}} \quad (7)$$

where *i* is the period of immersion (when *i* = 1, it means the specimens are immersed for one week, in turn, i = 2, 3, 4, 5, 6 and 7, means the specimens are immersed for 2, 3, 5, 7, 10 and 15 weeks, respectively).

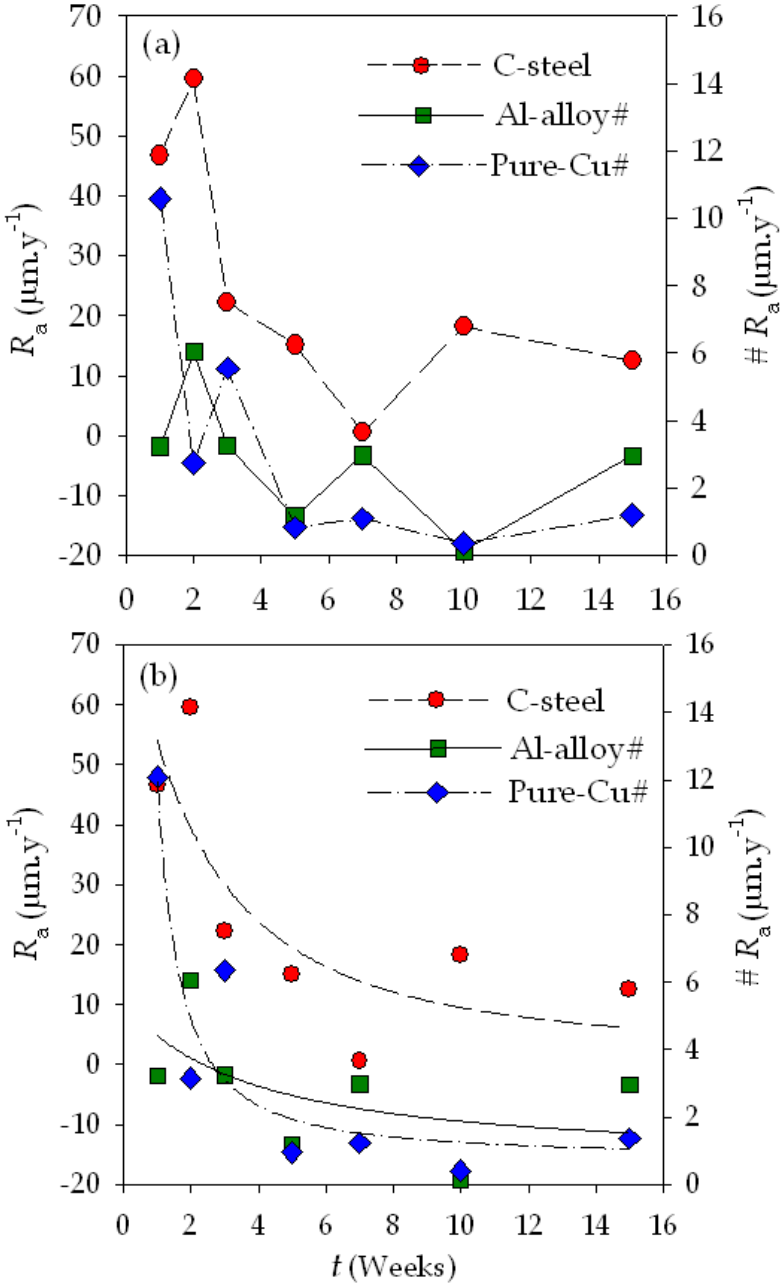

Figure 6. The variation of average corrosion rate of the studied metals as a function of immersion time in ROWE at room temperature (22 ± 1 °C).

The relation between the R_a value and the immersion time by weeks was plotted for C-steel, Al-alloy, and Pure-Cu as illustrated in Figure 6. It was found that R_a value fluctuates with immersion time (Figure 6-a), but approximate fitting for the data points reflects decreasing behavior for R_a with time (Figure 6-b). The decreasing of metal corrosion rate with exposure time was reported by several studies [35-37]. However, the fluctuation behavior of the average corrosion rate with time may be attributed to the so-called "Reverse Phenomenon" in which average corrosion rate reaches a minimum in a given period and then represents accretion trend [38].

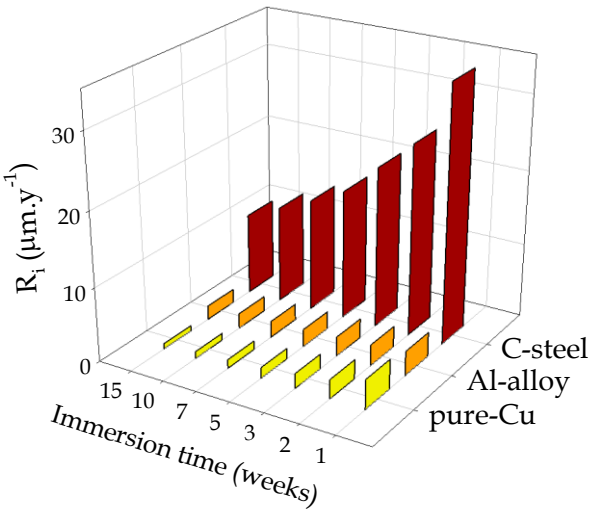

Figure 7. 3D relation between instantaneous corrosion rate, immersion time in ROWE and the metal type.

Unfortunately, the role of corrodent species is neglected when calculating the average corrosion rate and it depends on the weight difference before and after the exposure time. Hence, another quantity depends on the corrodent species can be calculated as follows [38]:

$$R_i = Knt^{n-1} \quad (8)$$

where R_i is the instantaneous corrosion rate, and it is the first derivative ($R_i = d\rho / dt$) of Eq. 2. Figure 7 represents the relation of three dimensions between the immersion period, the metal type and R_i value. Obviously, R_i value for the studied specimens gradually decreases with increasing immersion time, and no fluctuation trend is observed. It was found that the ratio between the value of R_i of the first week and that of the last week for C-steel, Al-alloy, and Pure-Cu are approximately 3, 2 and 6, respectively. This result indicates that the decrease in the corrosion rate with immersion time is powerfully related to the properties of the corrosion products formed on the metal surface. Therefore, Pure-Cu shows the highest decreasing ratio and the lowest *n* value (Table 4) which reflects a highly protective surface film as discussed before. Generally, the instantaneous corrosion rates of the studied metals give the same order that obtained from the thickness loss rate (*K*, Table 4).

3.2.3. Surface morphology by visual and microscopic inspection

A couple of photographs were obtained before, and after pickling for C-steel, Al-alloy and Pure-Cu immersed for three different periods in ROWE at room temperature and were illustrated in Figure 8. By visual inspection, general corrosion was observed for C-steel and Pure-Cu while pitting behavior was associated with Al-alloy corrosion. Before pickling, black corrosion products covered uniformly the C-steel surface while brown materials accumulate around the specific area on Al-alloy surface. The surface of Pure-Cu alloy does not change significantly before and after pickling as compared with C-steel and

Al-alloy, indicating good corrosion resistance for Pure-Cu which agrees well with rate measurements.

The surface morphology of the studied specimens after ten weeks of immersion in ROWE at room temperature was investigated using SEM technique and was illustrated in Figs. 9-11. It was observed that the surface features vary considerably according to the metal type. Table 5 summarized the main remarks for the surface of the studied specimens under the studied conditions.

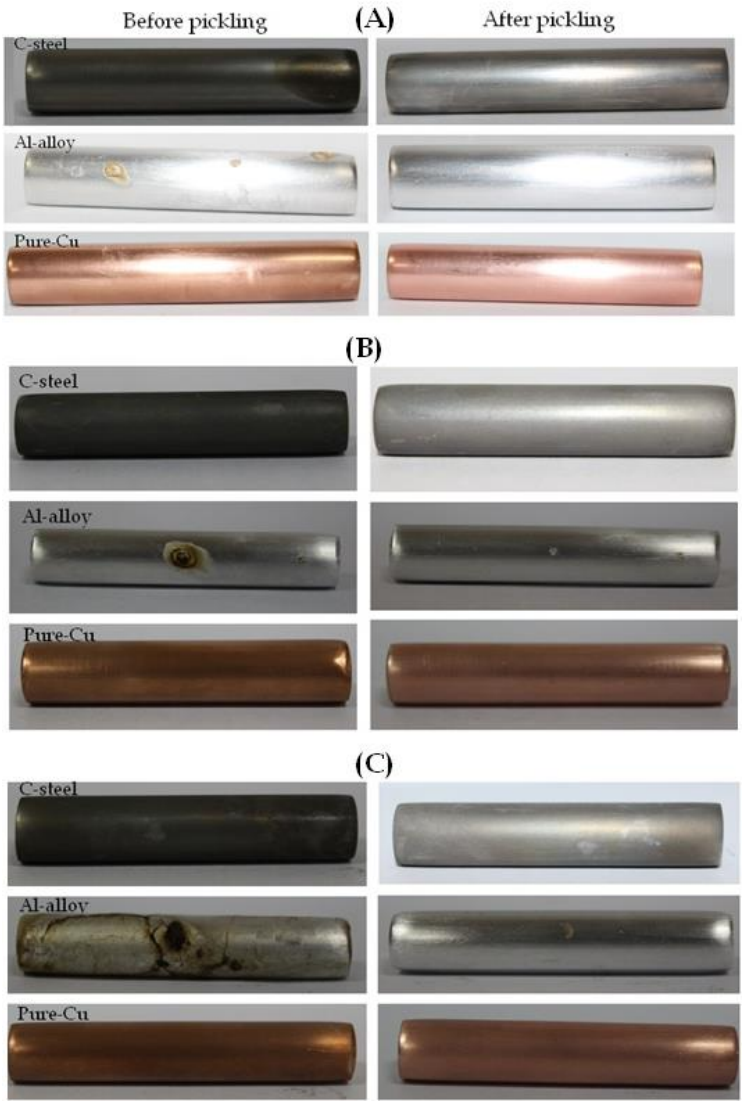

Figure 8. Optical photographs for the surface of C-steel, Al-alloy and Pure-Cu before and after pickling for (A) 1 week, (B) 3 weeks and (C) 10 weeks of immersionin ROWE at room temperature (22 ± 1 °C).

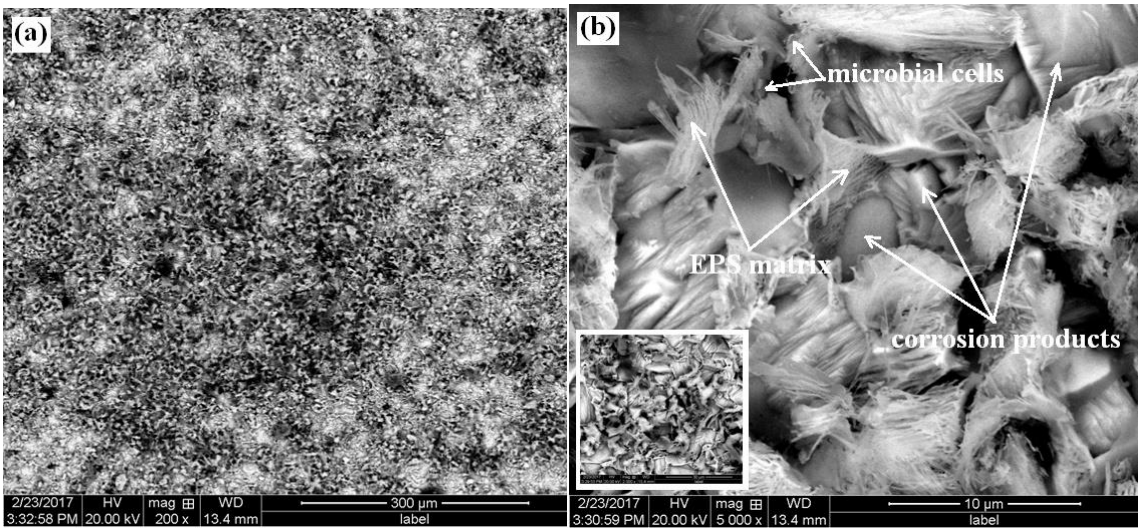

Figure 9. SEM micrographs with different magnifications (a: 300 ηm and b: 10 ηm) for C-steel surface obtained afterten weeks of immersion in ROWE at room temperature (22 ± 1 °C).

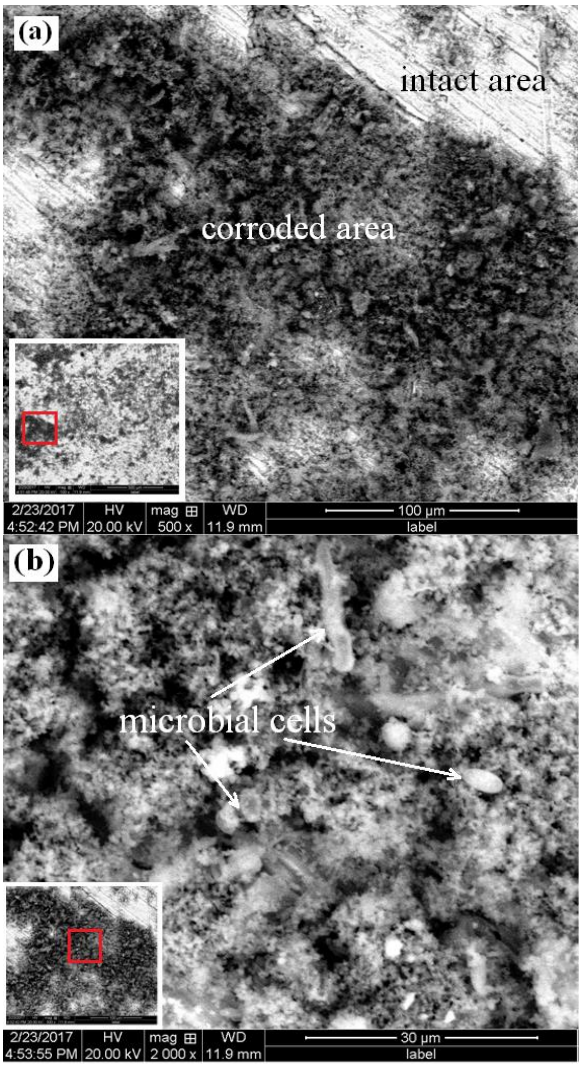

Figure 10. SEM micrographs with different magnifications (a: 100 ηm and b: 30 ηm) for Al-alloy surface obtained after ten weeks of immersion in ROWE at room temperature (22 ± 1 °C).

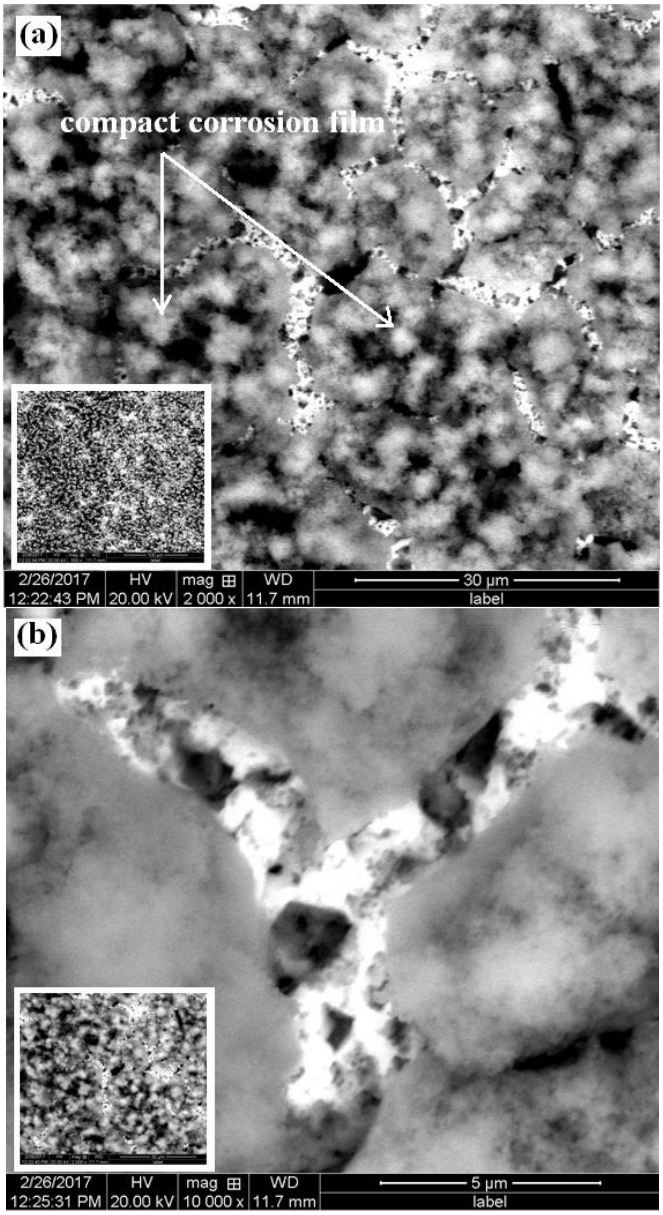

Figure 11. SEM micrographs with different magnifications (a: 30 ηm and b: 5 ηm) for Pure-Cu surface obtained after ten weeks of immersion in ROWE at room temperature (22 ± 1 °C).

Table 5. Surface features for C-steel, Al-alloy and Pure-Cu after immersion in ROWE for 10 weeks at room temperature (22 ± 1 °C).

C-steel	Al-alloy	Pure-Cu
Corrosion products distributed uniformly on the surface (general corrosion)	Corrosion products distributed randomly on the surface(localized corrosion) even some area shows the scratching marks of polishing process	Corrosion products distributed uniformly on the surface (general corrosion)

Corrosion products of high density and porosity	Porous corrosion products with density vary from area to area	Skinny compact corrosion products with micro cracking at its grain boundaries
Biofilm and microbial cells embedded within the corrosion products	Biofilm and microbial cells embedded within the corrosion products	Microbial activity is not detected

As was seen, corrosion can be concentrated locally (Figure 10) or can be extended across a wide area uniformly corroding the surface (Figure 9 and 11). Because diffusion controlled the corrosion process, higher corrosion rates reflect the more open structure of corrosion products (C-steel and Al-alloy) and vice versa. Accordingly, the morphology of Pure-Cu surface under the studied conditions is in good agreement with its kinetic corrosion parameters, i.e., the more compact corrosion layer gives the least corrosion rate as a consequence of its low diffusion coefficient. On the other hand, C-steel and Al-alloy obviously show microbial activity through the matrix of exopolysaccharidic substances (EPS) and the microbial cells that were observed on their surfaces, while it is not the case for the Pure-Cu specimen which showed no evidence of clear microbial activity. Porous natural materials such as wood are impossible to be kept completely clean and decontaminated. So, the microbial activity that observed in the case of C-steel and Al-alloy after ten weeks of immersion in ROWE was predictable. Microorganisms influence corrosion ranging from inducing localized corrosion, through a change in the rate of general corrosion, to corrosion inhibition [39]. Since a very active interaction between corrosion-product layers and biofilms can be expected, corrosion behavior of the metal varies depending on the extent of this mutual interaction [40]. According to the literature, the toxic and bactericidal properties of Cu^{2+} ions [41, 42] resist the bacteria growth and biofilm formation. The growth of bacteria in copper pipes has been shown to be slower than in other materials [43]. Moreover, laboratory assays have shown that cupric tannate (expected corrosion product) has a narcotic effect on biofouling larvae [44].

3.3. Electrochemical measurements at 30 ºC

Polarization curves for C-steel, Al-alloy, and Pure-Cu measured at 30 ºC in ROWE are given in Figure 12. Various electrochemical parameters were fitted from the polarization curves and are listed in Table 6, where β_c and β_a are cathodic and anodic Tafel slopes, i_{corr} is the corrosion current, andE_{corr} is the corrosion potential, respectively. Because polarization curve is characteristic of given combination of metal and environment, so the shape and the position of the polarization curves of different metals in certain environment depend on the nature of the electrochemical anodic and cathodic reactions and by the rate at which these reactions can proceed at the specific metal surface [45].Generally, on polarization from E_{corr} in the negative direction, the reduction reaction exercising activation polarization and hence Tafel behavior is obtained. At more active potentials the onset of polarization concentration phenomenon is observed. It is well known that the possible cathodic reactions in acid solutions containing oxygen are [46]:

hydrogen evolution $2H^+ + 2e^- \rightarrow H_2$ (9)

oxygen reduction $O_2 + 4H^+ + 4e^- \rightarrow 2H_2O$ (10)

In this case, the cathodic portion of the polarization curves may be the sum of two curves (hydrogen evolution and oxygen reduction) [47] and the concentration polarization region may be due to the lack of stirring and consumption the reactant species (O_2 and/or H^+) at the metal surface. On the other hand, the anodic curves show active metal dissolution portion (Eqs. 4-6) reflecting Tafel behavior which becomes limited at more positive potentials where the marked curvature is observed. The slowdown of current density with potential increase without showing passive behavior in the studied range of anodic potentials can be attributed to the fact that the corrosion process involves formation and re-dissolution of corrosion products, always maintaining the surface active [48]. Furthermore, another evident characteristic of Figure 12 is the position of Al-alloy curve appears nobler than that of C-steel. This behavior of Al-alloy is related to many factors, such as the type of alloying elements present in its microstructure (Table 1). It is evident that silicon is cathodic to the aluminum solid-solution matrix by several hundred of millivolts [49]. This cathodic alloying element may shift the corrosion potential of the alloy in the positive direction (more noble potentials). While the correlation between E_{corr} and corrosion possibility has not been specifically validated, but in the present work, the low E_{corr} values still suggest a high risk of corrosion (Table 6). It is reasonable to assess the corrosion behavior by estimating the i_{corr} to shore up the corrosion behavior obtained from E_{corr}[50]. According to i_{corr} values, the corrosion susceptibility of the studied metals can be given in the following order:

C-steel > Al-alloy > Pure-Cu

Figure 13 shows Nyquist plots for C-steel, Al-alloy, and Pure-Cu in ROWE solution at 30 ºC. Clearly, the capacitive arcs have different diameters depending on the corrosion resistance of each metal studied. Evidently, C-steel gives the lowest corrosion resistance. To estimate the EIS parameters such as polarization resistances and capacitances various equivalent circuits were tested to obtain the best one that fitted the experimental data. Two equivalent circuits were selected, one of them fits well the EIS data for both C-steel and Al-alloy (Figure 14a), and the other one fits well the EIS data for Pure-Cu (Figure14b). Where R_s is the solution resistance, R_{ct} and R_f are respectively the charge transfer, and the corrosion product film resistance and Q_{dl} and Q_f are the Constant Phase Element (CPE) for the double layer and the corrosion product film, respectively. At this point, CPE is frequently used to imply capacitance. In the real electrochemical systems, the pure capacitance is hardly measured due to surface roughness, heterogeneities or other effects that cause irregular current distribution over the metal surface [51]. The impedance of the CPE (Z_{CPE}) was expressed as [52]:

$$Z_{CPE} = \left[Q(j\omega)^n\right]^{-1} \quad (11)$$

Here, J is the imaginary unit and n is the exponent of the CPE and may vary between 0 and 1. For n=1, Eq. 11 implies the impedance of the ideal capacitor, so Q is defined as the real capacity C. For n<1, the real capacity can be calculated according to the following equation [53]:

$$C = Q^{1/n} R^{(1/n)-1} \quad (12)$$

According to Eq. 12, n value should be more than 0.75 to obtain C values with reasonable confidence. Obviously, the equivalent circuit is shown in Figure 15b indicates that the film formed on the pure-Cu surface has an important role in the corrosion process because its resistance was included as one of the simulated parameters (R_f). The fitting results are given in Tables 7 and 8. The R_s has values

in the range of 0.526-0.586 kohm.cm^2. R_s is related to the physicochemical changes of the wood extract around the studied metal during the experiment. Since tannin/Fe^{2+}or Fe^{3+} complexes precipitated from the early stage of electrode immersion (Figure 3) in the ROWE, the highest value of R_s was recorded for C-steel/ROWE system. R_{ct} values reflect that the studied metals have corrosion rates follow a similar trend to that obtained from WL and PDP measurements.

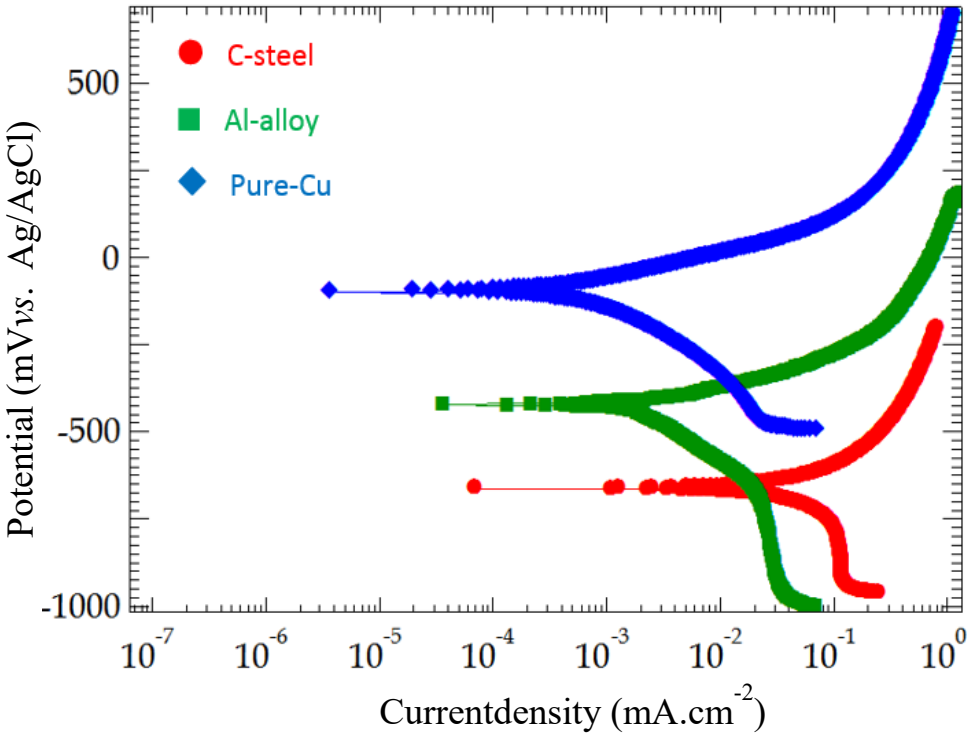

Figure 12. PDP curves for the corrosion of C-steel, Al-alloy and Pure-Cu in in ROWE at 30 oC.

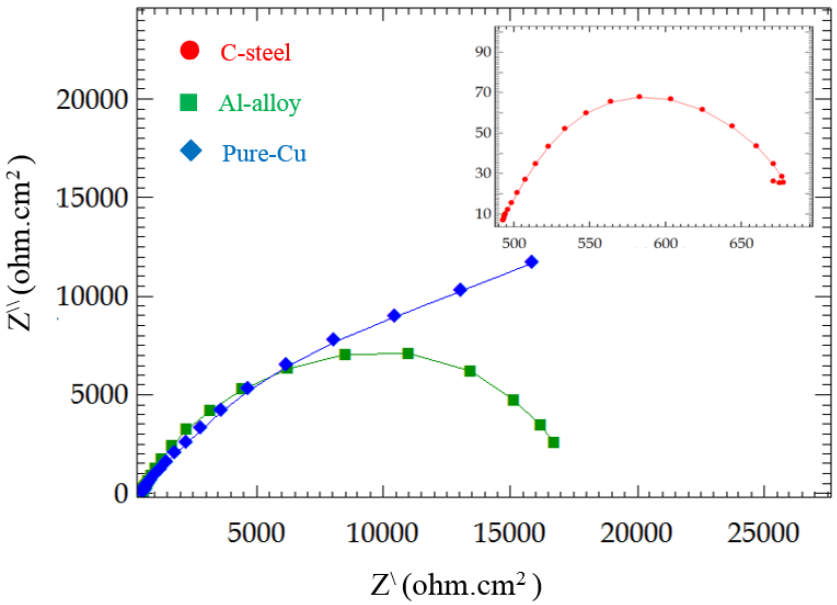

Figure 13. Nyquist plots for the corrosion of C-steel, Al-alloy and Pure-Cu in in ROWE at 30 ºC.

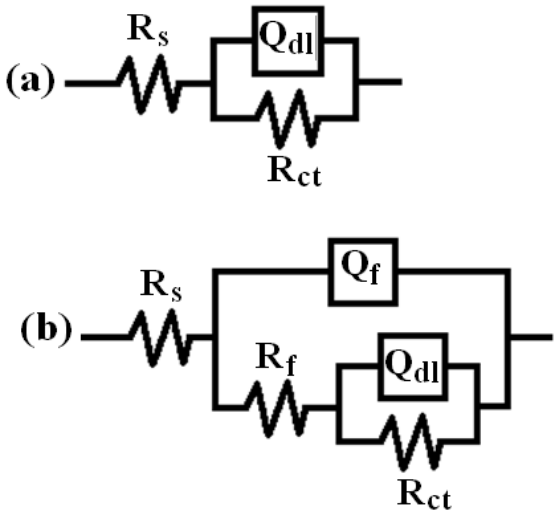

Figure 14. Equivalent circuits to simulate the EIS data obtained for (a) C-steel and Al-alloy and (b) Pure-Cu in ROWE.

Table 6. PDP parameters for the corrosion of C-steel, Al-alloy and Pure-Cu in ROWE at 30 °C.

Metal type	β_a (mV.dec^{-1})	$-\beta_c$ (mV.dec^{-1})	$i_{corr}\times10^3$ (mA.cm^{-2})	E_{corr} (mV)
C-steel	121.12	108.06	37.83 ± 2.00	-673.15
Al-alloy	74.28	190.13	1.52 ± 0.07	-429.75
Pure-Cu	69.45	108.77	0.55 ± 0.14	-97.63

Table 7. EIS parameters for the corrosion of C-steel and Al-alloy in ROWE at 30 °C.

Metal type	R_s (kohm.cm^2)	$C_{dl}\times10^5$ (F.cm^{-2})	n	R_{ct} (kohm.cm^2)	$\chi^2\times10^4$
C-steel	0.586	2.12	0.99	0.166 ± 0.023	3.09
Al-alloy	0.526	1.17	0.81	18.220 ± 0.043	9.14

Table 8. EIS parameters for the corrosion of Pure-Cu in ROWE at 30 °C.

Metal type	R_s (kohm.cm^2)	$C_f\times10^5$ (F.cm^{-2})	n	R_f (kohm.cm^2)	$C_{dl}\times10^5$ (F.cm^{-2})	n	R_{ct} (kohm.cm^2)	$\chi^2\times10^4$
Pure-Cu	0.545	0.89	0.80	2.171	7.54	0.49	54.210	3.89

4. CONCLUSIONS

The interaction between metal surface and the ROWE was observed visually where the color and clarity of the studied metal/ROWE systems depends on the type of the metal ion exist in the solution through the experiment duration. The WL data of the studied metals fit well the kinetic power law relation. According to the thickness loss after one year of immersion and the instantaneous corrosion rate, the following order for the studied metals can be obtained:

C-steel > Al-alloy > Pure-Cu

The exponent n of the kinetic model varied with the metal studied and the recorded value (n < 0.5) for Pure-Cu indicated good protective film properties. Visually, general corrosion could be distinguished for C-steel and Pure-Cu while pitting corrosion for Al-alloy. Microscopically, open structure corrosion film was detected which distributed uniformly on C-steel surface or locally on Al-alloy surface, while compact corrosion film was observed on Pure-Cu surface. Moreover, microscopic inspection indicated microbial activity on the corroded surface of the studied metals except for Pure-Cu. The electrochemical study revealed that with increasing both E_{corr} and R_{ct} the value of i_{corr} was decreased and hence the corrosion risk for the studied metals follows the similar order as above. It was found that the corrosion product film plays a role as a protective layer for Pure-Cu since it gives significant value for R_f and this result is in good consistency with the WL data.

References

1. A. J. Baker, Corrosion of metals in preservative-treated wood, Forest Products Laboratory, (1987).
2. R. H. Farmer, Chemistry in the Utilization of Wood: Pergamon Series of Monographs on Furniture and Timber, Elsevier (2013).
3. R. D. Graham, M. Wilson and A. Oteng-Amoako, Wood-metal corrosion: an annotated survey, in, Corvallis, Or.: Forest Research Laboratory, School of Forestry, Oregon State University (1976).
4. M. J. Schofield, in Shreir's Corrosion, M. Graham, R. Lindsay, S. Lyon, T. Richardson, D. Scantlebury and H. Stott Editors, , Elsevier, Oxford (2010) p. 1323.
5. S. L. Zelinka, D. R. Rammer and D. S. Stone, *Corros.Sci*., 50 (2008)1251.
6. S. L. Zelinka, R. J. Sichel and D. S. Stone, *Corros.Sci*., 52 (2010) 3943.
7. S. L. Zelinka and D. S. Stone, *Corrosion (2010)*, NACE International, Houston, TX, Paper No.: 10082, (2010).
8. S. Zelinka and D. Stone, Mater. Corros., 62 (2011)739.
9. S. L. Zelinka, D. Derome and S. V. Glass, *Build Environ*., 46 (2011) 2060.
10. S. L. Zelinka and D. R. Rammer, *Forest Prod J*., 62 (2012)160.
11. S. L. Zelinka, S. V. Glass and D. Derome, *Corros.Sci*., 83 (2014) 67.
12. S. L. Zelinka, S. V. Glass, C. R. Boardman and D. Derome, *Corros.Sci*., 102 (2016)178.
13. S. L. Zelinka, J. E. Jakes, G. T. Kirker, D. Vine and S. Vogt, in NACE CORROSION Conference & Expo Paper No. 9017.. (2017) 8 p.
14. G. Kear, H.-Z. Wú and M. S. Jones, , *Mater. Struct*., 41 (2008) 1405.
15. G. Kear, H.-Z. Wú, M. S. Jones and F. C. Walsh, *J. Appl. Electrochem*., 38 (2008) 1599.
16. G. Kear, H. Z. Wu and M. S. Jones, *Corros.Sci.,*51 (2009) 252.
17. ASTM Standard G1-90, Standard Practice for Preparing Cleaning and Evaluating Corrosion Test Specimens, in Philadelphia, PA, USA, (2000).
18. E. A. Noor and A. H. Al-Moubaraki, *J. Sci. Eng*., 39 (2014) 5421.
19. E. Sjostrom, Wood chemistry: fundamentals and applications, Elsevier (2013).
20. J. D. Hem, Complexes of ferrous iron with tannic acid, in USGPO, (1960).
21. P. South and D. Miller, *Food Chem*., 63 (1998) 167.
22. B. H. Cruz, J. M. Díaz-Cruz, C. Ariño and M. Esteban, *Electroanalysis*, 12 (2000) 1130.
23. P. Kraal, B. Jansen, K. G. Nierop and J. M. Verstraten, *Chemosphere,*65 (2006) 2193.
24. Y. Hu, R. Xu, J. Dynes, R. Blyth, G. Yu, L. Kozak and P. Huang, *Geochim. Cosmochim. Ac*., 72 (2008) 1959.
25. T. Okuda, K. Mori, M. Shiota and K. Ida, Yakugaku zasshi: *Journal of the Pharmaceutical Society of Japan*, 102 (1982) 735.

26. N. Slabbert, in Plant polyphenols, Springer, (1992) p. 421
27. M. Benarie and F. L. Lipfert, *Atmos. Environ*., 20 (1986) 1947.
28. S. Sun, Q. Zheng, D. Li and J. Wen, *Corros.Sci*., 51 (2009) 719.
29. E. A. Noor, *Mater. Corros*., 62 (2011) 786.
30. A. H. Al-Moubaraki, A. Al-Judaibi and M. Asiri, *Int. J. Electrochem. Sci*, 10 (2015) 4252.
31. C. Pan, W. Lv, Z. Wang, W. Su, C. Wang and S. Liu, *J. Mater. Sci. Technol*. 33 (2017) 587.
32. M. Morcillo, B. Chico, I. Díaz, H. Cano and D. De la Fuente, *Corros.Sci*., 77 (2013) 6.
33. R. E. Ricker, *J. Res. Natl. Inst. Stand. Technol*., 115 (2010) 373.
34. A. M. Beccaria and E. Mor, *Br. Corros. J.,*11 (1976) 156.
35. R. Vera, B. Rosales and C. Tapia, *Corros.Sci*., 45 (2003) 321.
36. S. Li, S. Jung, K.-w. Park, S.-M. Lee and Y.-G. Kim, *Mater. Chem. Phys*., 103 (2007) 9.
37. E. E. Ikechukwu and E. O. Pauline, *Open Journal of Social Sciences*, 3 (2015) 143.
38. Y. Ma, Y. Li and F. Wang, *Corros.Sci*., 52 (2010) 1796.
39. H. A. Videla and L. K. Herrera, *Int. Microbiol*., 8 (2005) 169.
40. A. Milling, R. Kehr, A. Wulf and K. Smalla, *Holzforschung*, 59 (2005) 72.
41. J. Trevors and C. Cotter, *J. Ind. Microbiol*., 6 (1990) 77.
42. C. L. Dupont, G. Grass and C. Rensing, *Metallomics*, 3 (2011) 1109.
43. M. J. Lehtola, I. T. Miettinen, M. M. Keinänen, T. K. Kekki, O. Laine, A. Hirvonen, T. Vartiainen and P. J. Martikainen, *Water Res*., 38 (2004) 3769.
44. M. Pérez, G. Blustein, M. García, B. del Amo and M. Stupak, *Prog. Org. Coat*., 55 (2006) 311.
45. W. Sluijter and P. Kreijger, *Heron*, 22 (1977) 13.
46. E. Bardal, Corrosion and Protection, Springer-Verlag, London, (2004).
47. H. J. Flitt and D. P. Schweinsberg, *Corros.Sci*., 47 (2005) 2125.
48. M. Veloz and I. González, *Electrochim. Acta,*48 (2002) 135.
49. J. R. Davis, Corrosion of aluminum and aluminum alloys, Asm International, (1999).
50. M. Franco, T. H. Krishna, A. M. Pillai, A. Rajendra and A. Sharma, *Acta Metall. Sin.-Engl*.,26 (2013) 647.
51. M. Palomar-Pardave, I. Gonzales, M. Romero-Romo, T. Oropez and M. Palomar-Pardave, Electrochemical Society: Pennington, NJ, USA, (2008).
52. F. F. Eliyan, E.-S. Mahdi and A. Alfantazi, *Corros.Sci,* 58 (2012) 181.
53. S. Sarker, A. Ahammad, H. W. Seo and D. M. Kim, *Int. J. Photoenergy*, (2014).